Acta Radiologica Open
8(3) 1–8

DOI: 10.1177/2058460119834690
journals.sagepub.com/home/arr
SAGE

Computer-aided pancreas segmentation based on 3D GRE Dixon MRI: a feasibility study

Xiaoliang Gong[1,*], Chao Ma[2,*], Panpan Yang[2], Yufei Chen[1], Chaolin Du[1], Caixia Fu[3] and Jian-Ping Lu[2]

Abstract

Background: Pancreas segmentation is of great significance for pancreatic cancer radiotherapy positioning, pancreatic structure, and function evaluation.

Purpose: To investigate the feasibility of computer-aided pancreas segmentation based on optimized three-dimensional (3D) Dixon magnetic resonance imaging (MRI).

Material and Methods: Seventeen healthy volunteers (13 men, 4 women; mean age = 53.4 ± 13.2 years; age range = 28–76 years) underwent routine and optimized 3D gradient echo (GRE) Dixon MRI at 3.0 T. The computer-aided segmentation of the pancreas was executed by the Medical Imaging Interaction ToolKit (MITK) with the traditional segmentation algorithm pipeline (a threshold method and a morphological method) on the opposed-phase and water images of Dixon. The performances of our proposed computer segmentation method were evaluated by Dice coefficients and two-dimensional (2D)/3D visualization figures, which were compared for the opposed-phase and water images of routine and optimized Dixon sequences.

Results: The dice coefficients of the computer-aided pancreas segmentation were 0.633 ± 0.080 and 0.716 ± 0.033 for opposed-phase and water images of routine Dixon MRI, respectively, while they were 0.415 ± 0.143 and 0.779 ± 0.048 for the optimized Dixon MRI, respectively. The Dice index was significantly higher based on the water images of optimized Dixon than those in the other three groups (all P values < 0.001), including water images of routine Dixon MRI and both of the opposed-phase images of routine and optimized Dixon sequences.

Conclusion: Computer-aided pancreas segmentation based on Dixon MRI is feasible. The water images of optimized Dixon obtained the best similarity with a good stability.

Keywords

Magnetic resonance imaging, pancreas, segmentation, Dixon

Received 11 November 2018; accepted 28 January 2019

Introduction

The incidence of pancreatic disease including pancreatic cancer, severe acute pancreatitis, and chronic pancreatitis increased. Pancreatic cancer is one of the highest mortality rate cancers (1,2). Early detection, accurate assessment, and appropriate treatment are critical for the disease. Most patients with clear clinical symptoms already have tumors, with only about 15% patients suitable for surgery. About 80% of patients died within one year of diagnosis, with a five-year survival rate < 5% (3). Severe acute pancreatitis can be found in young and middle-aged adults, with a high mortality

[1]College of Electronic and Information Engineering, Tongji University, Shanghai, PR China
[2]Department of Radiology, Changhai Hospital of Shanghai, The Second Medical University, Shanghai, PR China
[3]Application Development, Siemens Shenzhen Magnetic Resonance Ltd., Shenzhen, PR China

*Equal contributors.

Corresponding author:
Jian-Ping Lu, Department of Radiology, Changhai Hospital of Shanghai, The Second Medical University, No. 168 Changhai Road, Shanghai 200433, PR China.
Email: cjr.lujianping@vip.163.com

rate. The pain and malnutrition associated with chronic pancreatitis severely affect the quality of life of patients. Early diagnosis, treatment plan, and therapeutic effect evaluation of various diseases is of great significance based on the computer-aided diagnosis (CAD) method (4,5). Accurate pancreas segmentation based on radiographic images of a normal pancreas is the basis of the detection of image features of various pancreatic diseases. Computed tomography (CT) and magnetic resonance imaging (MRI) are the most common medical imaging tools for organ segmentation using CAD methods (6). Pancreas segmentation is of great significance for pancreatic cancer radiotherapy positioning (4), pancreatic structure, function evaluation (5), and so on.

MRI has become increasingly important in the diagnosis and evaluation of various abdominal diseases in clinical practice, thanks to its advantages of non-ionizing radiation and multiple soft-tissue contrasts (T1-weighted [T1W] imaging, T2-weighted [T2W] imaging, diffusion-weighted imaging [DWI], etc.). The use of MRI for tissue and organ computer segmentation is to be studied; some researchers have proposed several abdominal organ segmentation approaches based on MRI images. The shape, size, and location of pancreases differ greatly among individuals and visceral fat around the pancreas can drastically vary the boundary contrast as well. With CT images, the accuracy of pancreatic segmentation is significantly lower than that of other abdominal organs (7,8). Similar phenomena were found based on a two-dimensional (2D) MRI of two volunteers (9). Partial volume effect may be contributed by several types of surrounded organs (10), which can introduce the uncertainty of qualify analysis based on digital images, such as MRI, positron emission tomography (PET), and so on (11,12). A high performance of pancreas segmentation remains a challenging task.

Some pancreas segmentation works were focused on developing new segmentation algorithms to overcome the low-contrast problem of pancreas in the routine medical images. Shimizu et al. reported that the Jaccard index (JI) of an automatic segmentation pancreas method was about 57.9% based on three-dimensional (3D) contrast-enhanced CT (13). Gou et al. utilized a hybrid gradient, region growth, and shape constraint (hGReS) method to segment a 2D upper abdominal dynamic MRI (dMRI) and achieved 0.770 (9). Later, Gou et al. developed a novel dictionary learning (DL) method to segment based on T2W half-Fourier acquisition single-shot turbo spin-echo (HASTE) and T1W volumetric interpolated breath-hold examination images (14). These methods were tested on three patients and two healthy volunteers. However, the study of the method should be considered on a larger sample size.

The 3D gradient echo (GRE) Dixon sequence is commonly used in clinical abdominal MRI examinations. It can simultaneously obtain the in-phase, opposed-phase, water, and fat MR images (15). The 3D GRE Dixon has remarkable advantages in high spatial resolution and good soft-tissue contrast. In most cases, the water images from 3D GRE Dixon acquisition can provide a clear anatomical structure of the pancreas and its boundary and is widely used in pancreas MRI examinations (16). In addition, threshold is one of the most effective segmentation methods. In past decades, many threshold techniques have been presented for medical image analysis (17–19). Image processing operators based on classical mathematical morphology (20) have been widely used in medical image analysis and processing (21). Recently, some advanced morphological processing operators have been proposed and it is used in medical image processing, such as blood vessel segmentation (22,23).

Thus, in this study, we prospectively investigated the feasibility and stability of computer-aided pancreas segmentation based on the Medical Imaging Interaction ToolKit (MITK) software platform, with the traditional segmentation algorithm (a threshold method and a morphological method), using 3D GRE Dixon images, which were optimized in the slice thickness to reduce the partial volume effect.

Material and Methods

Participants

This prospective study was approved by our Institutional Review Board. Signed written informed consent was obtained from all participants after detailed explanation and before imaging. Seventeen healthy volunteers (13 men, 4 women; mean age = 53.4 ± 13.2 years; age range = 28–76 years) were enrolled in this study between October 2016 and November 2016.

MRI

All examinations were performed on a 3.0-T MR scanner (MAGNETOM Skyra, Siemens Healthcare, Erlangen, Germany) with an 18-element phased array coil. All patients underwent routine pancreatic MRI sequences, including the routine VIBE (Volume Interpolation Breath-hold Exam, 3D GRE) DIXON sequence and its optimized protocol specified for pancreas segmentation. The parameters of the routine

VIBE DIXON were: TR = 3.97 ms; TE = 1.26/2.49 ms; acquisition matrix = 320 × 196; field of view (FOV) = 400 × 325 mm; number of slices = 64; slice thickness = 6 mm; flip angle = 9°; total scan time = 15 s in one breath-hold. The parameters for the optimized VIBE Dixon protocol were as follows: TR = 3.92 ms; TE = 1.23/2.46 ms; acquisition matrix = 288 × 188; FOV = 400 × 325 mm; number of slices = 40; slice thickness = 3 mm; slice gap = 0 mm; flip angle = 9°; total scan time = 18 s in one breath-hold.

Data analysis

The four image sets from VIBE Dixon, including opposed-phase, in-phase images, water, and fat images, were automatically reconstructed inline. Two radiologists independently evaluated the image quality on the feasibility of showing the boundary of the pancreas and selected the qualified ones for pancreas segmentation.

The manual segmentation of the pancreas was based on the (http://www.mitk.org/), which is a free, open-source software system for the development of interactive medical image processing software. MITK combines the Insight Toolkit (ITK; http://www.itk.org/) and the Visualization Toolkit (VTK; http://www.vtk.org/) with an application framework. A trained radiologist (with eight years of experience in abdominal radiology and two years of experience in imaging manual segmentation) manually drew free-hand regions of interest (ROIs) to include all pancreatic tissue on water and opposed-phase Dixon images separately by using MITK; the integral area of each slice of the manual segmentation of pancreas was automatically recorded.

The computer-aid segmentation is based on the Otsu threshold method (24) and a morphological method. They were executed on the MITK platform with a useful tool button. The working pipeline was implemented as follows:

- import MRI data into the MITK platform;
- select the ROI of the input image by a cutting button to reduce the computation cost;
- use the Otsu threshold method (24) for fast segmentation of the images, resulting in binary images.

The threshold method is simple and easy to implement; it plays an important role in image segmentation (25,26). Ideally, this method is to divide the given image into two classes: foreground and background. The Otsu method is a popular method for optimal global threshold processing. By choosing the threshold value k to maximize the variance between foreground and background, the new image $f(x, y)$, a binary image, is defined as

$$f(x,y) = \begin{cases} 1 & \text{if } g(x,y) \geq k \\ 0 & \text{if } g(x,y) < k \end{cases} \quad (1)$$

1. Carrying out a mathematical morphology analysis, a technique for extracting the geometrical structures of the binary images is done by twice erosion operations and then twice dilation operation on the binary images. The aims of the morphological operation were to isolate different organs, remove the adhesion of organs, and fill holes in the binary images.

The mathematical morphology is a regular method for the extraction of image composition, image preprocessing, and image post-processing. Dilation and erosion are two basic morphological operations. Erosion can remove areas of an object that do not contain the structuring element, break thin connections, removes thin protrusions, and smooth the object outline. Dilation can join narrow breaks, fill up holes smaller than the structuring element, and smooth the object contours by filling up narrow gulfs. In image processing applications, the operations of dilation and erosion are most commonly used in a variety of combinations.

The erosion and dilation are defined in term of set operations. The erosion of A by B, denoted as $A \ominus B$, is defined as

$$A \ominus B = \{z | B_z \subseteq A\} \quad (2)$$

where set A is a set in Z^2 and B is a structuring element. Essentially, the erosion of A by B is the collection of the origin positions of all structural elements, where the conversion B does not overlap with the background of the A.

The dilation of A by B, denoted as $A \oplus B$, is defined as

$$A \oplus B = \left\{ z \middle| (\hat{B})_z \cap A \neq \varnothing \right\} \quad (3)$$

where $\varnothing$ is empty. In other words, the dilation of A by B is the set consisting of all the structuring element origin locations where the reflected and translated B has overlapped at least some parts of A.

2. Select the region of pancreas then remove the remaining parts.
3. 3D reconstruction of the pancreas using the segmentation results.

Validation of the segmentation

The performance of our proposed computer segmentation method was evaluated by the similarity between the binary mask images generated by the automatic segmentation and the manual ground truth segmentation by the radiologist, represented by Dice coefficient (27):

$$\mathrm{DI} = 2\frac{|\mathrm{A1} \cap \mathrm{A2}|}{|\mathrm{A1}| + |\mathrm{A2}|} \quad (4)$$

where A1 and A2 represent binary mask images from the proposed method and manual segmentation, respectively. $\mathrm{DI} > 0.7$ indicates a high similarity between the two segmentation results (28).

Statistical analysis

Statistical analyses were performed by using SPSS software (Version 16.0, SPSS Inc., Chicago, IL, USA). Comparisons of the achieved Dice coefficients based on different image groups were performed by using the Wilcoxon signed-rank test. A P value < 0.05 is statistically significant.

Results

Two trained radiologists evaluated the feasibility of pancreas segmentation based on the image qualities and clear boundary of the pancreas. The radiologists agreed that both the opposed-phase and water images of both VIBE Dixon sequences showed a clearer boundary of the pancreas than in-phase and fat images. In the study, the opposed-phase and water images of VIBE Dixon sequences achieved by the routine (slice thickness = 6 mm) and optimized (slice thickness = 3 mm) parameters were compared to investigate the feasibility and stability of computer-aided pancreas segmentation based on MITK with 17 volunteers. The performances of the computer-aided pancreas segmentation method introduced in this study were evaluated by Dice coefficients. Then 2D and 3D figures were used to assess visually the performances of segmentation.

Segmentation similarity based on Dixon images

Dice coefficients between our segmentation method and radiologist manual ground truth segmentation of the routine Dixon opposed-phase and water images were 0.633 ± 0.080 and 0.716 ± 0.033, respectively. The difference was statistically significant ($P < 0.001$) (Table 1).

Dice coefficients of our method and manual ground truth based on the optimized opposed-phase and water images were 0.415 ± 0.143 and 0.779 ± 0.048, respectively. The difference was statistically significant ($P < 0.001$) (Table 1). Dice coefficients of pancreas segmentation based on the routine Dixon water images were significantly lower than those based on the optimized image groups ($P < 0.001$). Based on opposed-phase images, only 4/17 cases from routine images and 1/17 case from optimized images achieved $\mathrm{DI} > 0.70$. While comparing the routine Dixon water images, which had 11/17 (65%) cases, 16/17 (94%) cases of the optimized Dixon water phase images achieved $\mathrm{DI} > 0.70$. The water images from the optimized VIBE Dixon improved the segmentation effectiveness.

Table 1. Dice coefficients of computer segmentation for routine and optimized Dixon images.

	Routine Dixon images		Optimized Dixon images	
Case no.	Oppose phase	Water phase	Oppose phase	Water phase
1	0.531	0.684	0.488	0.699
2	0.565	0.693	0.298	0.785
3	0.611	0.765	0.110	0.840
4	0.672	0.723	0.489	0.772
5	0.587	0.726	0.312	0.783
6	0.675	0.762	0.494	0.840
7	0.806	0.787	0.741	0.826
8	0.641	0.721	0.325	0.802
9	0.735	0.724	0.525	0.827
10	0.575	0.666	0.349	0.767
11	0.646	0.681	0.541	0.808
12	0.572	0.676	0.464	0.706
13	0.511	0.705	0.458	0.710
14	0.662	0.723	0.516	0.752
15	0.549	0.691	0.287	0.713
16	0.722	0.718	0.338	0.811
17	0.695	0.728	0.327	0.799
Mean	0.633	0.716	0.415	0.779
SD	0.080	0.033	0.143	0.048

2D visualization of pancreas segmentation based on Dixon images

The example segmentation results of the head, body, and tail of the pancreas, based on routine/optimized Dixon water images and opposed-phase images, are shown in Figs. 1 and 2, respectively. Based on Dixon water images, the automatic segmentation results worked very well for the pancreatic head, body, and tail.

3D visualization of pancreas segmentation

The reconstructed 3D images of six pancreas segmentation results based on optimized water Dixon images are illustrated in Fig. 3. Our segmentation method

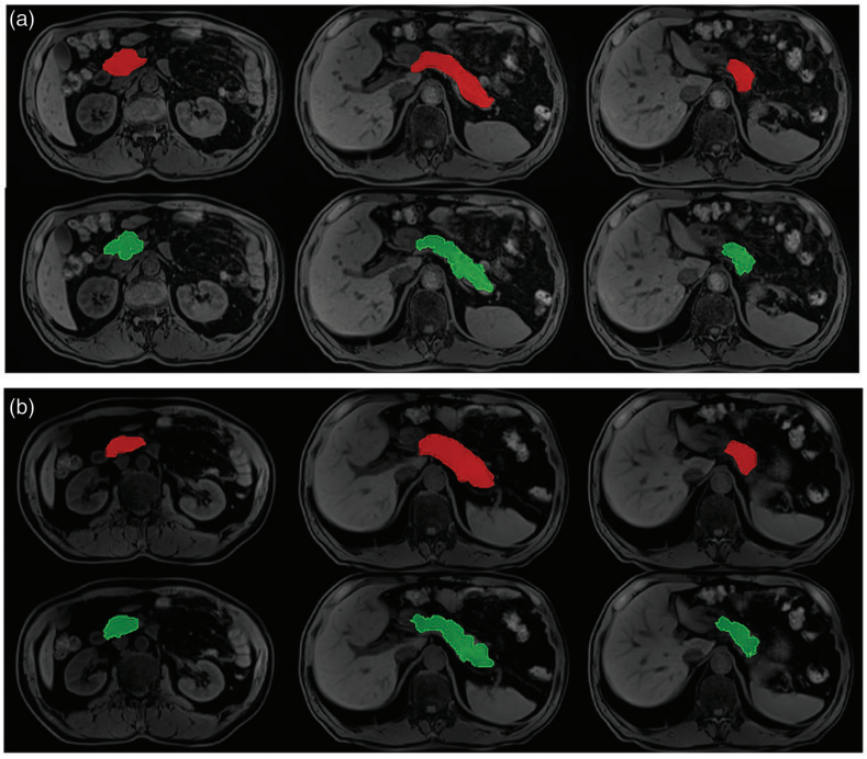

Fig. 1. Example results from automatic segmentation (green) and manual ground truth (red) segmentation based on optimized (a) and routine (b) Dixon water images, respectively.

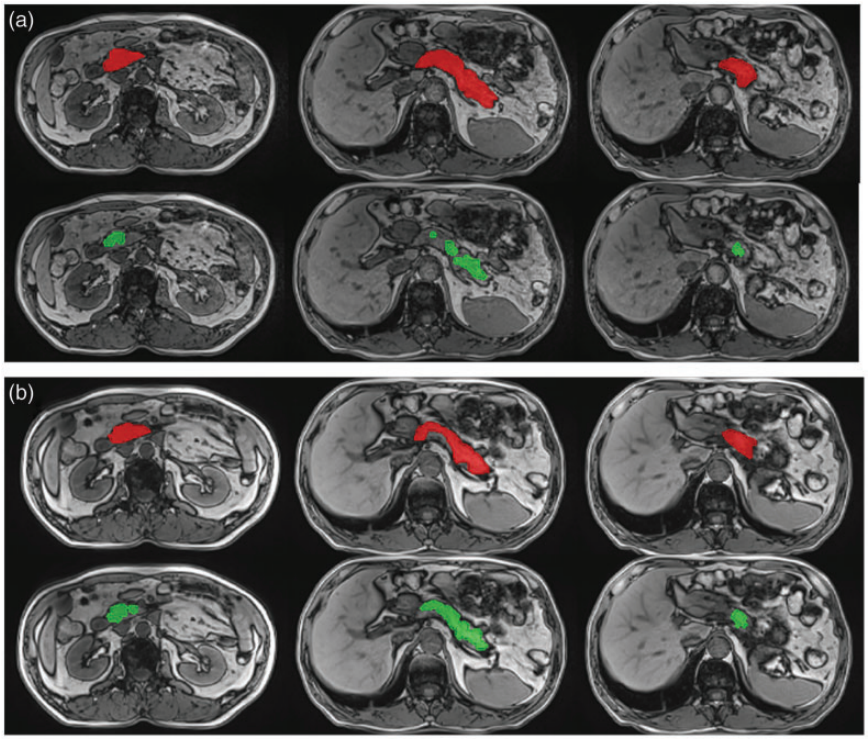

Fig. 2. Example results from automatic segmentation (green) and manual ground truth (red) segmentation based on optimized (a) and routine (b) Dixon opposed-phase images, respectively.

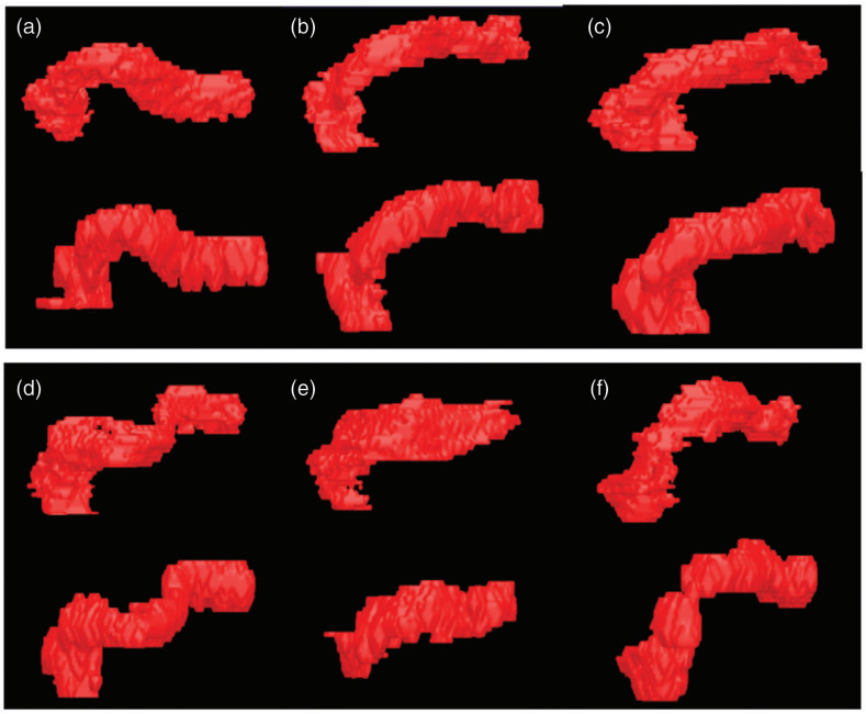

Fig. 3. 3D segmentation results by automatic segmentation and manual ground truth of different ages based on optimized Dixon water phase images, respectively. (a) DI = 0.811; (b) DI = 0.808; (c) DI = 0.826; (d) DI = 0.802; (e) DI = 0.772; (f) DI = 0.799.

results visually matched very well with the manual ground truth.

Discussion

Accurate automatic segmentation of the pancreas is helpful to MR-guided radiotherapy for pancreatic cancer (9). In the current study, we proposed a computer-aided pancreas segmentation method based on the software platform MITK with the traditional segmentation algorithm (a threshold method and a morphological method) which is simple and easy for widespread use. Utilizing the water images of the VIBE Dixon sequence, our segmentation method performed very well on the pancreas.

Good image quality, including sufficient signal-to-noise ratio (SNR) and contrast and spatial resolution, are prerequisites for successful segmentation. The Dixon technique used in this study was able to separate water and fat perfectly; the pancreas can be delineated clearly in the water images. In addition, the spatial resolution in slice direction was increased by 100% to 3 mm for the optimized Dixon protocol in this study, while the in-plane spatial resolution was decreased by 15% to partially compensate the loss of the SNR due to the decreased thickness. The trained radiologists visually evaluated the four image sets from VIBE Dixon opposed-phase, in-phase images, water, and fat images. To save the computational costs, two kinds of images, including the opposed-phase and water images of VIBE Dixon sequences, were focused on, based on the radiologist agreements. The resulting images of the optimized VIBE Dixon, especially the water images, have better spatial resolution and sufficient SNR, which help to obtain better results for pancreas segmentation.

A previous study reported computer-assisted pancreas segmentation based on 2D or 3D CT images (13), but the accuracy of pancreas segmentation is significantly lower than that of other abdominal organs (8). The main reason is that the pancreas is located in the depths of the upper abdomen and its surrounding tissues are relatively complex. In addition, the position of the pancreas varied in different individuals. MRI is an important tool to detect and characterize pancreatic diseases, with good soft-tissue contrast superior to CT (29). Shen et al. (5) proposed a method of automatic segmentation of abdominal organs based on the fat images from 3D Dixon sequence; the average Dice coefficient for 20 obese patients was 0.672. In the current study, based on the water images of the optimized Dixon, the automatic pancreas segmentation using our method obtained excellent similarity (the mean Dice coefficient was 0.779 and the standard deviation was 0.048). This suggested that the water images of 3D

Dixon might better than fat images for CAD segmentation of the pancreas which met the agreements of the radiologists by a visual evaluation. Gou et al.'s (14) newest research results show that they acquired a Dice coefficient > 0.83 from 12 imaging volumes from three patients and two healthy volunteers, while the results obtained in our study were based on 17 healthy volunteers. It is noticed that the optimized Dixon water images that reduced the slice thickness could obtain more stable segmentation performance even based on the traditional threshold and morphological method.

This study had some limitations. First, the main limitation was that the number of participants was limited and all cases were healthy volunteers. Further studies with a larger sample size including patients with chronic pancreatitis, diabetes, and cancer should be included to assess the lesion detection performance of the software. Second, the manual user interaction step was required to modify the automated segmentation results by removal of other unrelated organizations. This step does not require high precision and it takes very little time to accomplish whole pancreas segmentation. Future automatic pancreas segmentation methods should be developed.

In conclusion, it was found that computer-aided pancreas segmentation based on the traditional segmentation algorithms pipeline was feasible when using the water images of 3D Dixon. The water images of the optimized Dixon which reduced the slice thickness to relieve the partial volume effect achieved the best similarity with a good stability.

Acknowledgements

The authors thank Dr. Xiaoying Shan, Dr Xu Yan and Mr. Luguang Chen provided technical help in the study.

Declaration of conflicting interests

The authors declared no conflicts of interest with respect to the research, authorship, and/or publication of this article.

Funding

The authors disclosed receipt of the following financial support for the research, authorship, and/or publication of this article: This work was supported by the Science and Technology Innovation Action project (174119552200), Natural Science Foundation of Shanghai (16JC1401300), Natural Science Foundation of China (81601468 and 61573235), and Precision Medical Transformation Application project of SMMU (2017JZ42).

ORCID iD

Chao Ma http://orcid.org/0000-0002-2473-387X

References

1. Rahib L, Smith BD, Aizenberg R, et al. Projecting cancer incidence and deaths to 2030: the unexpected burden of thyroid, liver, and pancreas cancer in the United States. *Cancer Res* 2014;74:2913–2921.
2. Ferlay J, Parkin DM, Steliarova-Foucher E. Estimates of cancer incidence and mortality in Europe in 2008. *Eur J Cancer* 2010;46:765–781.
3. Hidalgo M, Cascinu S, Kleeff J, et al. Addressing the challenges of pancreatic cancer: Future directions for improving outcomes. *Pancreatology* 2015;15:8–18.
4. Crijns SP, Raaymakers BW, Lagendijk JJ. Proof of concept of MRI guided tracked radiation delivery: Tracking one-dimensional motion. *Phys Med Biol* 2012;57:7863–7872.
5. Shen J, Baum T, Cordes C, et al. Automatic segmentation of abdominal organs and adipose tissue compartments in water-fat MRI: Application to weight-loss in obesity. *Eur J Radiol* 2016;85:1613–1621.
6. Höhne KH, Hanson WA. Interactive 3D segmentation of MRI and CT volumes using morphological operations. *J Comput Assist Tomogr* 1992;16:285–294.
7. Sørensen, T. A method of establishing groups of equal amplitude in plant sociology based on similarity of species and its application to analyses of the vegetation on Danish commons. *Kongelige Danske Videnskabernes Selskab*. 1948;5:1–34.
8. Chu C, Oda M, Kitasaka T, et al. Multi-organ segmentation based on spatially-divided probabilistic atlas from 3D abdominal CT images. *Med Image Comput Comput Assist Interv* 2013;16:165–172.
9. Gou S, Wu J, Liu F, et al. Feasibility of automated pancreas segmentation based on dynamic MRI. *Br J Radiol* 2014;87:20140248.
10. Tohka J. Partial volume effect modeling for segmentation and tissue classification of brain magnetic resonance images: A review. *World J Radiol* 2014;6:855–864.
11. Vos SB, Jones DK, Viergever MA, et al. Partial volume effect as a hidden covariate in DTI analyses. *Neuroimage* 2011;55:1566–1576.
12. Soret M, Bacharach S L, Buvat I. Partial-volume effect in PET tumor imaging. *J Nucl Med* 2007;48:932–945.
13. Shimizu A, Kimoto T, Kobatake H, et al. Automated pancreas segmentation from three-dimensional contrast-enhanced computed tomography. *Int J Comput Assist Radiol Surg* 2010;5:85–98.
14. Gou S, Lee P, Hu P, et al. Feasibility of automated 3-dimensional magnetic resonance imaging pancreas segmentation. *Adv Radiat Oncol* 2016;1:182–193.
15. Dixon WT. Simple proton spectroscopic imaging. *Radiology* 1984;153:189–194.
16. Ma J. Dixon techniques for water and fat imaging. *J Magn Reson Imaging* 2008;28:543–558.
17. Sathya PD, Kayalvizhi R. Optimal segmentation of brain MRI based on adaptive bacterial foraging algorithm. *Neurocomputing* 2011;74:2299–2313.
18. Maitra M, Chatterjee A. A novel technique for multilevel optimal magnetic resonance brain image thresholding using bacterial foragin. *Measurement* 2008;41:1124–1134.

19. Manikandan S, Ramar K, Iruthayarajan MW, et al. Multilevel thresholding for segmentation of medical brain images using real coded genetic algorithm, *Measurement* 2014;47:558–568.
20. Gonzalez RC, Woods RE. *Digital Image Processing*. Englewood Cliffs, NJ: Prentice-Hall, 2002.
21. Cline HE, Thedens DR, Meyer CH, et al. Combined connectivity and a gray-level morphological filter in magnetic resonance coronary angiography. *Magn Reson Med* 2000;43:892–895.
22. Bouraoui B, Ronse C, Baruthio J, et al. 3D segmentation of coronary arteries based on advanced mathematical morphology techniques. *Comput Med Imaging Graph* 2010;34:377–387.
23. Dufour A, Tankyevych O, Naegel B, et al. Filtering and segmentation of 3D angiographic data: Advances based on mathematical morphology. *Med Image Anal* 2013;17:147–164.
24. Otsu N. A threshold selection method from gray-level histogram. *IEEE Trans* 1979;9:62–66.
25. Chen YB, Chen TC. Image segmentation method using thresholds automatically determined from picture contents. *EURASIP J Image Video Process* 2009;1:1–15.
26. Navon E, Miller O, Averbuch A. A color image segmentation based on adaptive local thresholds. *Image Vision Comput* 2005;23:69–85.
27. Truong QB, Lee BR. Automatic multi-thresholds selection for image segmentation based on evolutionary approach. *Int J Control Autom* 2013;11:834–844.
28. Zijdenbos AP, Dawant BM, Margolin RA, et al. Morphometric analysis of white matter lesions in MR images: Method and validation. *IEEE Trans Med Imaging* 1994;13:716–724.
29. Frampas E, David A, Regenet N, et al. Pancreatic carcinoma: Key-points from diagnosis to treatment. *Diagn Interv Imaging* 2016;97:1207–1223.